



ORIGINAL ARTICLE

Nitrate removal from aqueous solution using watermelon rind derived biochar-supported ZrO₂ nanomaterial: Synthesis, characterization, and mechanism



Huy Hoang Phan Quang^a, Kiet Tuan Phan^a, Phong Dinh Lam Ta^a, Nga Thi Dinh^b, Taghrid S. Alomar^c, Najla AlMasoud^c, Chao-Wei Huang^{d,*}, Ankush Chauhan^e, Van-Huy Nguyen^{f,*}

^a Faculty of Biology and Environment, Ho Chi Minh City University of Food Industry, 140 Le Trong Tan Street, Tay Thanh Ward, Tan Phu District, Ho Chi Minh City, Vietnam

^b Research Institute for Sustainable Development, Ho Chi Minh University of Natural Resources and Environment, 236B Le Van Sy Street, Ward 1, Tan Binh District, Ho Chi Minh City, Vietnam

^c Department of Chemistry, College of Science, Princess Nourah bint Abdulrahman University, Riyadh 11671, Saudi Arabia

^d Department of Engineering Science, National Cheng Kung University, No. 1, Daxue Rd., East Dist., Tainan 701401, Taiwan

^e Faculty of Allied Health Sciences, Chettinad Academy of Research and Education (CARE), Kelambakkam, Kanchipuram district-603103, Tamil Nadu, India

^f Chettinad Hospital and Research Institute, Chettinad Academy of Research and Education (CARE), Kelambakkam, Kanchipuram district-603103, Tamil Nadu, India

Received 17 May 2022; accepted 4 July 2022

Available online 8 July 2022

KEYWORDS

Nitrate;
ZrO₂;
Biochar;
Watermelon rind;
Pyrolysis

Abstract Recently, biochar has attracted tremendous research interest for environmental applications. In this study, biochar-derived watermelon rind (WM) was produced via optimal pyrolysis at 500 °C for 2 h, and then improved the adsorption capacity by Zirconium oxide nanoparticles (ZrO₂ NPs). The WM@ZrO₂ was characterized using X-ray diffraction (XRD), Scanning electron microscopic - Energy-dispersive X-ray spectroscopy (SEM-EDS), and Fourier transform infrared (FTIR). The adsorptive capacities of synthesized ZrO₂ NPs were investigated for nitrate as a function of pH, adsorbent dosage, contact time, initial adsorbate concentration, and pyrolysis temperature in the batch experiment. The results showed that a Langmuir isotherm and a

* Corresponding authors.

E-mail addresses: huangcw@gs.ncku.edu.tw (C.-W. Huang), vhnguyen.ChE@gmail.com (V.-H. Nguyen).

Peer review under responsibility of King Saud University.



pseudo-second-order kinetics model were the best-fit for experimental nitrate data in its non-linear form as correlation coefficients (R^2) were 0.985 and 0.998, respectively. The maximum adsorption capacity for the Langmuir isotherm model was 15.196 mg g⁻¹. The proposed mechanism, including electrostatic attraction and ligand exchange, played a dominant role in nitrate adsorption. After testing with the real domestic wastewater, the removal of nitrate for WM@ZrO₂ was achieved at 78 %, which was equivalent to the adsorption capacity of 8.1 mg g⁻¹ of adsorbent. Overall, the WM@ZrO₂ is proposed as a promising, effective, and environmentally friendly adsorbent in removing nitrate from an aqueous solution.

© 2022 The Authors. Published by Elsevier B.V. on behalf of King Saud University. This is an open access article under the CC BY-NC-ND license (<http://creativecommons.org/licenses/by-nc-nd/4.0/>).

1. Introduction

Nitrate-contaminated water or wastewater has become a critical problem due to the widespread use of nitrogen fertilizers, a severe threat to human health and the environment, and the improper management of wastewater from industrial sites (Li et al., 2010). Nitrates can be converted to nitrites, which react with haemoglobin to generate methaemoglobin, leading to being fatal to newborns (Gupta et al., 2000). Moreover, nitrate in drinking water could cause methemoglobinemia, carcinoma, and malformation (Majumdar and Gupta 2000). Thus, nitrate treatment in water and wastewater is emerging for the sustainable removal of such contaminants.

Solid organic wastes have paid more attention due to the urbanization and industrialization process (Chen et al., 2020). Among them, agricultural wastes were classified as solid organic wastes, which could proceed with potential environmental problems such as foul odors (H₂S, C₂H₆S, etc.), the number of intensive livestock, pathogenic microorganisms, leaching of harmful and other pollutants into groundwater (Dai et al., 2018). Additionally, agricultural waste has a loose, porous structure, and contains many functional groups (e.g., carboxyl, hydroxyl) and other reactive groups, which could be used as biomass adsorption material (Dai et al., 2018). Hence, extensive agricultural waste disposal significantly improves environmental pollution control, leading to an environmentally friendly methodology. Therefore, the utilization of locally abundant watermelon rind as agricultural organic wastes has been employed to contribute to the “treating waste by waste” (Guo et al., 2020).

Adsorption treatment is commonly utilized in water treatment due to its simplicity, low cost, and simple process (Varsha et al., 2022). Recent adsorbents such as nanoparticles (NPs) (Tyagi et al., 2018), fibrous chitosan (Zhuang et al., 2022), organic resins (Li et al., 2020), mineral-based (Chen et al., 2020), and nanostructured carbon (Liu et al., 2018) have been applied to remove contaminants from water. However, the drawbacks of these adsorbents lead to a limit to their practical applications owing to the high-cost adsorbents and complicated synthesis process. Therefore, it is essential to develop the adsorbent through a simple synthesis process, which is low in cost and has a technically feasible application. Due to its inexpensive cost, abundant raw materials (i.e., organic waste, crops, animal manure, etc.), and excellent adsorbent, biochar seems to be a more useful and promising adsorbent (Zhang et al., 2017). Biochar is a carbon-rich material formed by pyrolyzing waste materials such as wood, poultry litter, and crop residues (Almaroai et al., 2014). Biochar has been developed as an enhanced pore structure, a large specific surface area, and large surface functional groups, and is regarded as an excellent adsorption material (Luo et al., 2022). Using biochar is less investment in operational cost, simple design, and basic operation, especially with no toxic substances (Long et al., 2019, Yu et al., 2022). In addition, biochar has been increasingly utilized to remove organic and inorganic pollutants from contaminated water (Wang et al., 2017). At present, a great deal of research has been researched on agricultural waste to adsorb heavy metals and organic pollutants (Yadav et al., 2021). In consequence, the development of biochar with effective adsorbent,

low-cost, simple operation, and environmentally friendly become more meaningful.

Many studies have recently focused more on zirconium-based adsorbents because of their superior anion adsorption capabilities. Zirconium oxide (ZrO₂) is a non-hazardous, commercially sustainable, and long-lasting metal with several applications such as oxygen sensors and electrolytes for fuel cells, and heavy metal sequestration (Alagarsamy et al., 2022). The use of ZrO₂ NPs in contaminated water with nitrate may positively contribute to water and wastewater management (Quang et al., 2022). Various adsorbent using ZrO₂ was applied for improving adsorption capacities from ZrO₂-based drinking water sludge for nitrate anions removal (Quang et al., 2022), Nanohybrid composite Fe₂O₃-ZrO₂/Black cumin (BC) for arsenic and dyes removal (Siddiqui and Chaudhry 2019), ZrO₂ decorated nitrogen-rich azacytosine tethered graphene oxide-based dendrimer for arsenite removal (Prabhu et al., 2019), and ZrO₂ coated ball-milled coal fly-ash magnetic spheres (Zhang et al., 2020) for phosphate removal. However, the adsorption research of inorganic anions like nitrate on ZrO₂-based biochar as watermelon rind is comparatively fewer.

The novelty of this work is to dope ZrO₂ NPs onto biochar-derived watermelon rind (WM) in order to modify the properties of WM for enhancing nitrate adsorption capacity by purely green methodology in the pyrolysis process and to evaluate its application in the removal of nitrate from an aqueous solution. In addition, the utilization of agricultural waste for biochar will solve waste by waste with high environmental significance. Hence, the present study is focused on (i) the synthesis of WM@ZrO₂; (ii) the effect of different parameters, including pyrolysis temperature, pH, initial concentration, adsorbent dosage, and contact time; (iii) understanding the mechanisms of nitrate removal on the biochar; (iv) feasibility of utilizing biochar-derived agricultural wastes.

2. Materials and methods

2.1. Chemicals

Analytical grade Zirconyl chloride (ZrO₂·8H₂O; 98% pure), sulfuric acid (H₂SO₄; 95–97% pure), sodium hydroxide (NaOH; 98% pure), hydrochloric acid (HCl; 95–99% pure) were all purchased from Shanghai Nanoport Company (Shanghai, China). The reagents and chemicals employed were all of the analytical grade. Double distilled water (DW) has been utilized for all experiment solutions.

2.2. Preparation of biochar

The watermelon rinds were sliced into tiny pieces, cleaned with DW, dried at 80 °C, crushed, and sieved using a standard sieve (No. 70) before the adsorption experiment. The pyrolysis furnace reactor was then fed with sieved samples and was per-

formed at 200, 300, 400, 500, and 600 °C with a heating rate of 5 °C min⁻¹ by the pyrolysis process. This process proceeded for 2 h after reaching the desired pyrolysis temperature. The biochar was then washed with DW and ethanol to remove harmful organic compounds from the biochar. The obtained biochar (called WM) was further dehydrated at 105 °C in the air oven and was stored in a vacuum desiccator for the further adsorption experiment. The chemical properties of WM are described in Table 1.

2.3. Preparation of ZrO₂-based biochar

Zirconyl solutions were prepared by adding ZrOCl₂·8H₂O (3.23 g) into 50 mL of deionized water to achieve a solution containing 0.2 mol L⁻¹ of Zr. To enhance adsorption capacity, about 3 g of biochar was homogeneously dispersed in 50 mL Zirconyl solutions, then 1 N NaOH solution was added drop by drop under mixing conditions with the rate of 450 rpm

for 12 h at ambient temperature to reach the solution pH to 10.5. After that, the precipitates were obtained and washed with DW and ethanol to eliminate chemicals. Finally, the sample is dried out for 12 h at 60 °C to obtain ZrO₂-based biochar. A schematic diagram for the fabrication of ZrO₂-based biochar (called WM@ZrO₂) is shown in Fig. 1.

2.4. Adsorption experiments

The nitrate (NO₃⁻) concentration was determined using the UV-Visible Spectrophotometric method (Shimadzu, Japan) with absorbance at 220 nm based on standard methods (4500-NO₃⁻ B). The batch experiments were carried out to evaluate the nitrate adsorption of WM and WM@ZrO₂. Nitrate standard solution was prepared in a concentration of 10–100 mg L⁻¹ from a stock solution (500 mg L⁻¹). The effect of pH (2–9), adsorbent dosage (10–50 mg), initial concentration (10–100 mg L⁻¹), and contact time (10–60 min) was investigated to find the optimal conditions with the maximum adsorption capacity. The desired adsorbent was placed in a 50 mL nitrate solution in a conical flask of 100 mL for a constant shaker with 200 rpm at 25 °C for 2 h. All the experiments were carried out in duplicates. The supernatant was separated by filtration using Whatman No. 1 filter paper, and then was analyzed for further experiment. The reusability experiment was conducted for five consecutive cycles. The equilibrium adsorption capacity of nitrate onto biochar was calculated as follows (Eq. (1)):

$$q_e = \frac{(C_o - C_e) \times V}{W} \quad (1)$$

where, C_o, C_e (mg L⁻¹) are concentrations of nitrate at the initial time and equilibrium, respectively; V (L) is the volume of solution, and W (g) is the weight of adsorbent.

Formula	Percentage (%)
Al ₂ O ₃	3.59
CaO	12.57
K ₂ O	11.19
P ₂ O ₅	6.74
Na ₂ O	2.48
MgO	5.22
SiO ₂	48.01
Fe ₂ O ₃	4.67
MnO	0.12
SO ₃	4.81
TiO ₂	0.52
ZnO	0.08

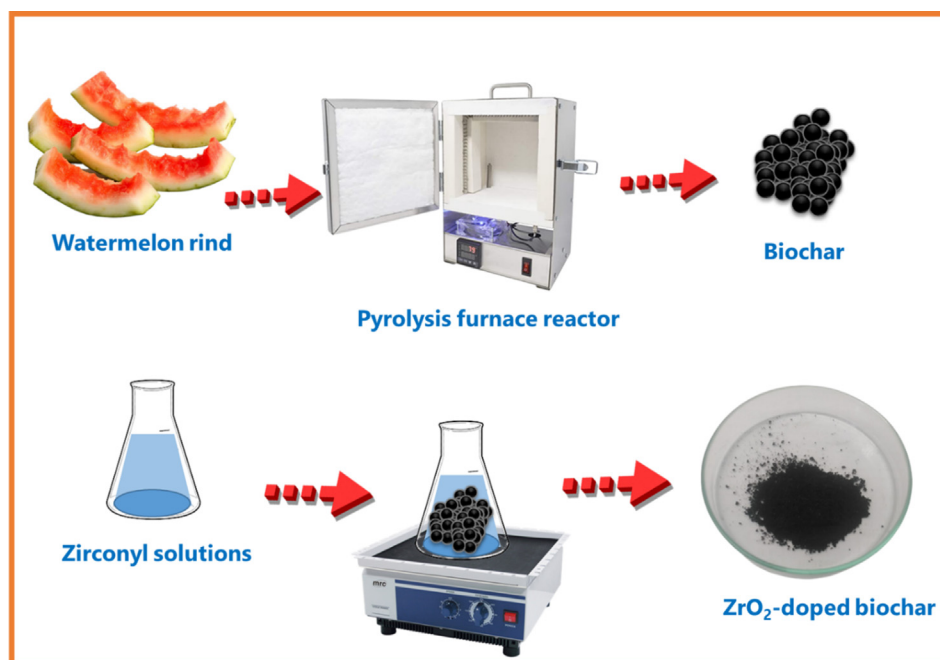


Fig. 1 A schematic diagram for fabrication of ZrO₂-based biochar.

The adsorption kinetics was utilized to interpret the sorption mechanisms using Pseudo-first-order, Pseudo-second-order, Elovich (Low 1960), and Intra-particle diffusion models (Weber Jr and Morris 1963). In contrast, various adsorption isotherm models were used, including Langmuir, Freundlich, Sips (Sips 1948), and Redlich-Peterson models (Redlich and Peterson 1959) of WM and WM@ZrO₂ for nitrate adsorption. The correlation coefficient (R^2) and chi-square test (χ^2) are fundamental parameters to determine the fitted experimental data (He et al., 2015).

2.5. Characterization of the adsorbents

BET (Brunauer–Emmett–Teller) surface area was carried out with SSA-4300. All the samples were analyzed by X-ray diffraction (XRD) using XRD D8 ADVANCE (Bruker) with the Cu K α radiation as the primary source, and it was conducted in the 2θ range of 5–80°. The microstructures were measured by Scanning electron microscopic (SEM) images using an energy-dispersive X-ray spectroscopy machine (S-4800, Hitachi, Japan) was used in order to evaluate the morphological changes on the adsorbent surface. The functional groups of biochar were analyzed by Fourier transform infrared (FTIR) spectroscopy (FTIR-6300 spectrophotometer) in the range of 4000–500 cm^{-1} wavelength, and the resolution was 4 cm^{-1} . X-ray fluorescence spectrometry (XRF) was used (ZSX Primus II, Rigaku, Japan). The pH drift method measured the point of zero charges (pH_{PZC}) (Khadhri et al., 2019).

2.6. Desorption of WM@ZrO₂

A desorption experiment was carried out for five consecutive cycles to evaluate the regenerative capability of WM@ZrO₂. The process for adsorbent regeneration included that saturated WM@ZrO₂ was dispersed in 1 M NaOH for the shaker at 200 rpm for 24 h, then filtered and washed with DW until neutral pH was obtained. Finally, the regenerated adsorbent was oven-dried at 80 °C for 2 h and was prepared for a subsequent cycle of adsorption-desorption experiment. For each cycle, 30 mg of WM@ZrO₂ was dispersed in 20 mg L^{-1} of initial nitrate concentration for 2 h with pH 2.

3. Results and discussion

3.1. Physicochemical characteristics of biochar

Biochar has a significant impact on the pees, such as BET surface area. The adsorbent's surface area in this study is 2.007 $\text{m}^2 \text{g}^{-1}$ which is suitable for the adsorption process. The proper pyrolysis temperature released intensively volatile matters and enhanced pores, high porosity, and surface area, resulting in a larger surface area (Liu et al., 2015).

The XRD patterns of biochar are shown in the 2θ values of 5–80° in Fig. 2a. The intensity of XRD spectra of biochar indicates that the main constituents belong to quartz (SiO₂) and calcite (CaCO₃). Some elements are enriched on the surface of biochar, such as salt ions (i.e., Na, K, Ca, Cl) during high pyrolytic biochar. This finding can be discussed further in section 3.6.

The FTIR spectra evaluate all functional groups of the surface of WM. FTIR of WM was shown in Fig. 2b. It was found that the board bands of FTIR spectra were between 4000 and 3600 cm^{-1} from stretching vibration of the O–H bond. A wide band at 2200 and 1600 cm^{-1} represented C \equiv C, C = O, and C = C bond stretching vibration.

Fig. 2c depicts an SEM analysis of WM. Herein, the rough surface and regular pores were identified in WM. The broadened pore diameter, increased surface porosity, and pore size could result in the formation of channel structures of WM during pyrolysis, most likely due to the surface thermal decomposition. Therefore, the improved surface structure is favorable for adsorption sites to adsorb more adsorbate onto the adsorbent surface.

3.2. Effect of pyrolysis temperature

One of the most suitable procedures for generating biochar is pyrolysis, which has greater energy density, lower moisture content, and bulk volume (Waqas et al., 2018). Fig. 2d depicts the effect of pyrolysis temperature on the nitrate adsorption capacity. As the pyrolysis increased from 200 to 500 °C, the adsorption capacity of WM@ZrO₂ yield increased remarkably from 9.8 ± 0.5 to $12.5 \pm 1.6 \text{ mg g}^{-1}$, respectively. This behavior is mainly due to the enhanced volatilization of organic matters in adsorbents, resulting in more ZrO₂-coated adsorption sites on the surface of adsorbents. In addition, the increased carbonation temperature could enhance adsorption capacity (Fan et al., 2020). Also, Cuixia et al. (2020) reported that the release of hemicellulose, cellulose, part of the lignin, surface functional groups, and loss of residual organic compounds occurred between 200 and 350 °C and 350–600 °C, respectively (Cuixia et al., 2020). Hence, the accelerated pyrolysis temperature significantly improved the performance of adsorption capacity, which is consistent with the results of another research (Zhao et al., 2019). However, further pyrolysis temperature may slightly decrease the nitrate adsorption capacity. This is probably due to the destruction of pore structures at higher temperatures and more formation of mesopores (Tan et al., 2015). Therefore, the pyrolysis temperature of WM was applied in this study at a pyrolysis temperature of 500 °C.

3.3. Effect of various adsorption parameters on biochar

pH is one of the significant fundamental factors that impact nitrate adsorption capacity. As shown in Fig. 3a, the nitrate adsorption capacity of biochar decreased with an increase in initial pH, and the highest adsorption capacity was achieved at pH 2, confirming that WM and WM@ZrO₂ were favorable for nitrate adsorption under acidic conditions. Specifically, the adsorption capacity decreased by 50 % as pH increased from 2 to 7, then continuously decreased to 1 mg g^{-1} as pH was obtained at 9. With a higher pH (pH > 7) from the neutral to alkaline condition, the competition adsorption between OH[−] and nitrate anions may occur in aqueous media by occupying the active sites of biochar (Zong et al., 2018), resulting in an abatement of adsorption capacity from 3.6 to 1 mg g^{-1} . This behavior was in good agreement with Zhang et al. (2020) reported that most ZrO₂-based adsorbents were favorable for acidic conditions, and the best condition was obtained at pH 2 (Zhang et al., 2020). The nitrate adsorption capacity in

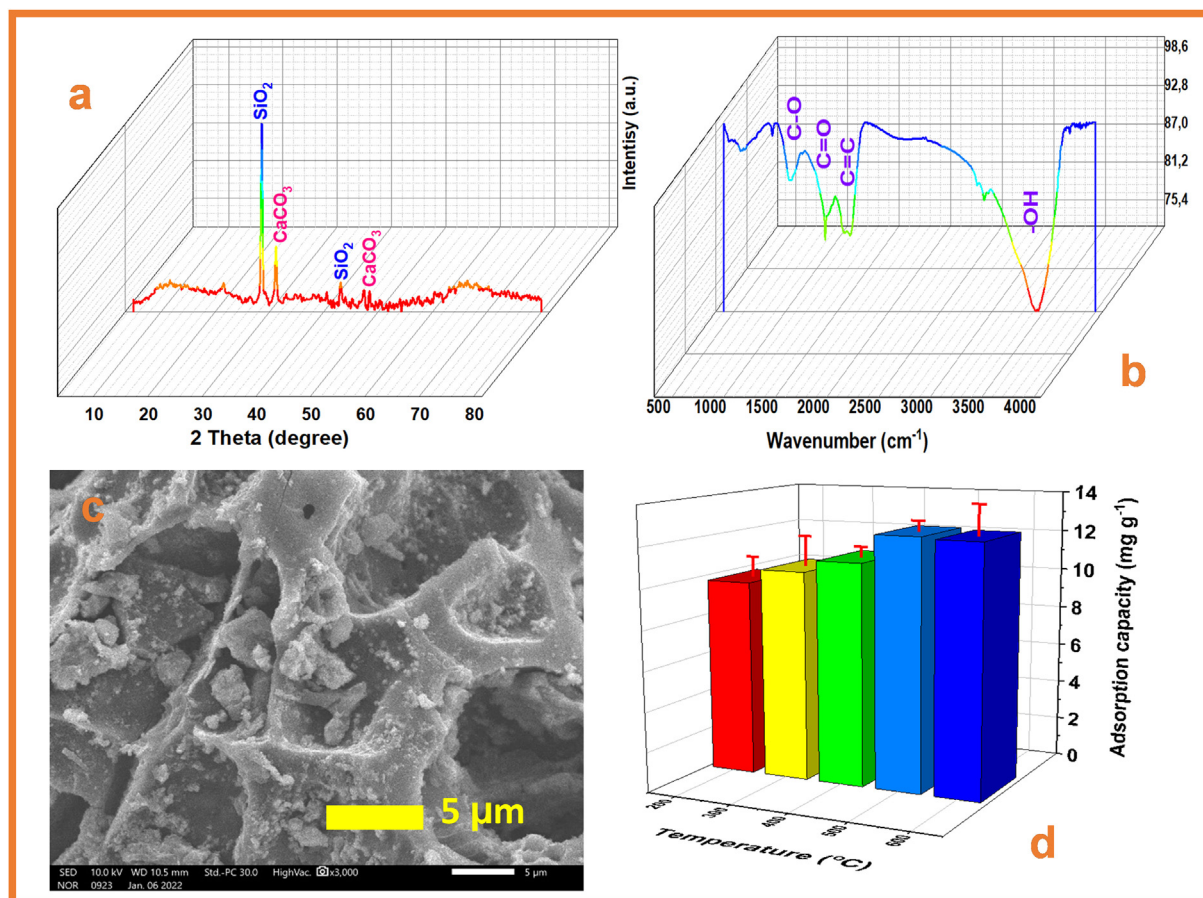


Fig. 2 Characteristics of watermelon rind (WM): (a) XRD patterns of WM, (b) FTIR spectra of biochar, (c) SEM images of WM, and (d) Pyrolysis temperature of WM@ZrO₂ on the adsorption capacity. (For interpretation of the references to color in this figure legend, the reader is referred to the Web version of this article.).

terms of pH can be accounted for the surface charge of biochar. This behavior will be further mentioned in the adsorption mechanism section.

As a critical parameter influencing adsorption performance, initial nitrate concentration remarkably impacted adsorption capacity. Fig. 3b depicts that the adsorption capacity increased in an increase in initial nitrate concentration due to the availability of a large surface area of the adsorbent. However, the multilayered surface interaction of active sites occurred in further adsorption reactions, leading to an unchangeable trend of adsorption capacity in further nitrate concentration.

The adsorption capacities of WM and WM@ZrO₂ in the impact of various adsorbent dosages were investigated. Fig. 3c depicts the adsorbent dosage in the performance of adsorption capacity. The adsorption capacities of biochar increased by increasing the adsorbent dosage owing to the available ZrO₂ NPs on the surface of the adsorbent. However, it was observed that the higher amount of adsorbent (> 30 mg) offered the equilibrium conditions thereby those of biochar slightly decreased. Similar results are also supported by Wong et al. (Wong et al., 2018).

Fig. 3d shows the reaction time of WM and WM@ZrO₂ during adsorption. The adsorption was sharply increased in the first 30 min, then proceeded slowly until the equilibrium condition was achieved as the adsorption and desorption of

adsorbent were obtained. The rapid adsorption at the initial contact time could be attributed to the abundant availability of ZrO₂ active adsorption sites on the surface of the adsorbent. The adsorption process then decreased slightly in the adsorption rate due to a relatively lower number of active sites.

3.4. Adsorption kinetics

The evaluation of adsorption kinetics is to understand the mechanism of adsorption, the factor relating to reaction rate, and to determine the suitable kinetics models. Four kinetics models have been studied to interpret the adsorption mechanism for nitrate. Reaction and diffusion-based kinetics models were performed, including Pseudo-first-order, Pseudo-second-order, Elovich, and Intra-particle diffusion models (see Fig. 4a). The kinetics parameters, correlation coefficients, and chi-square (χ^2) are shown in Table 2. Based on the correlation coefficients, the pseudo-second-order of biochar was the best fit for nitrate adsorption kinetics. This result implied that chemisorption was the rate-limiting step between the solid and liquid phases in the adsorption process (Zhao et al., 2019).

To investigate the diffusion mechanisms and rate-controlling procedure, the intra-particle diffusion was employed for the adsorption process on a porous adsorbent

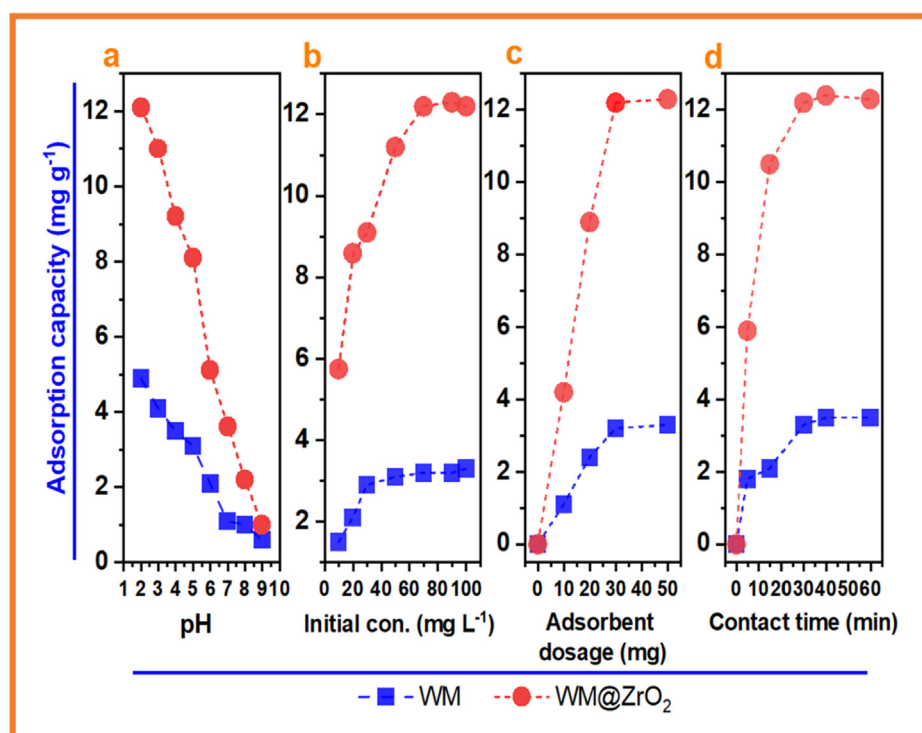


Fig. 3 Effect of the nitrate adsorption conditions of WM and WM@ZrO₂ on the adsorption capacity: (a) pH (Conditions: Initial concentration of nitrate: 20 mg/L; Adsorbent dose: 30 mg, Contact time: 30 min; Volume: 50 mL); (b) initial nitrate concentration (mg L⁻¹) (Adsorbent dose: 30 mg, pH 2; Contact time: 30 min; Volume: 50 mL); (c) the adsorbent dosage (mg) (Conditions: Initial concentration of nitrate: 20 mg/L; pH 2; Contact time: 30 min; Volume: 50 mL). The effect of adsorbent dosage is usually reported in (g L⁻¹), but it is formally in (mg) in this study; and (d) the contact time (min) (Conditions: Initial concentration of nitrate: 20 mg/L; Adsorbent dose: 30 mg, Contact time: 30 min; pH 2; Volume: 50 mL). (For interpretation of the references to color in this figure legend, the reader is referred to the Web version of this article.).

related to the transportation of species from an aqueous solution to a solid phase. The solid-solution transfer system has three stages: surface diffusion, intra-particle diffusion, and equilibrium dynamics processes (see Fig. 4a). These results were similar to Jedynak et al. that reported adsorption is not the only rate-limiting step for the entire process (Jedynak et al., 2019).

3.5. Adsorption isotherms

Fig. 4b illustrates the nitrate adsorption isotherm of WM and WM@ZrO₂. It can be realized that the WM@ZrO₂ exhibited a high adsorption capacity for nitrate, and the maximum adsorption capacity was based on the Langmuir model to be as high as 15.196 mg g⁻¹, which is closest to the maximum adsorption capacity of 12.278 mg g⁻¹ of experimental data (q_{exp}). The adsorption data were fitted with four isotherm models, including Langmuir, Freundlich, Sips, and Redlich-Peterson. The isotherm parameters, including correlation coefficients (R^2) and chi-square (χ^2), are summarized in Table 3. The maximum adsorption capacity of WM@ZrO₂ for nitrate was higher than that of WM for all the isotherm models. Specifically, to compare with WM, the maximum adsorption capacity of WM@ZrO₂ increased by 273 % in the Langmuir model, 254 % in the Freundlich model, 368 % in the Sips model, and 2123% in the Redlich-Peterson model. It is evident from the analysis that the best fitting of the Langmuir isotherm

model ($R^2 > 0.98$) confirms the monolayer adsorption at homogeneous adsorption sites on the surface of biochars. Dimensionless constant separation factor (R_L) of a solid-liquid adsorption system resulted in the favorable Langmuir adsorption system ($0 < R_L < 1$) (see Table 3). These results also indicate that the chemical was dominant in nitrate adsorption for WM and WM@ZrO₂.

3.6. The mechanism of adsorption

Micrograph scanning electron (SEM) is utilized to characterize the surface appearance and identify macro-pores of biochar. Fig. 5 depicts the magnification SEM micrograph of biochar before and after nitrate adsorption. WM@ZrO₂ exhibited likely a porous structure with smooth, tight, and rough surfaces on both biochar before (Fig. 5a, b) and after (Fig. 5c, d) nitrate adsorption, attributed to the chemical compositions of the biochar (Tanaka et al., 2015). Additionally, as shown in Fig. 5c, the ZrO₂ NPs on the surface of biochar may have an irregular shape. The properties of WM@ZrO₂, such as surface area and pores, have been improved as pyrolysis temperatures increased. This behavior was attributed to the internal release of volatile gas, the mineral crystallinity, and the formation of aromatic structures (Kim et al., 2012). In addition, the effect of N₂ gas in the pyrolysis processes for nitrate adsorption was omitted, whereas the majority of N content on the WM@ZrO₂ from nitrate in the aqueous solution was obtained

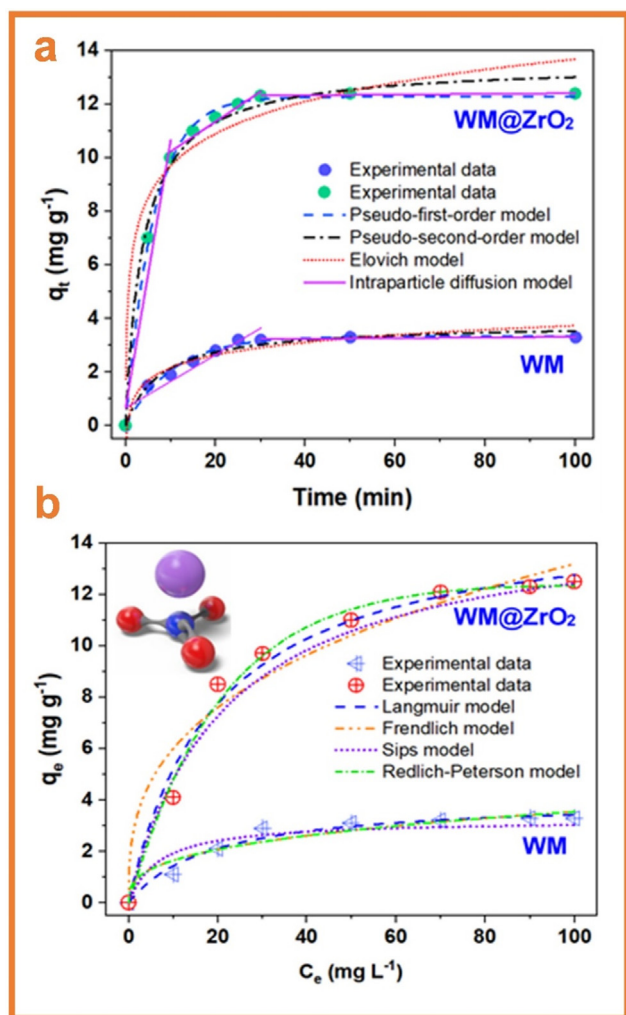


Fig. 4 (a) Different kinetics models for nitrate adsorption of WM and WM@ZrO₂, including Pseudo-first-order, Pseudo-second-order, Elovich, and Intraparticle diffusion models. (b) Different isotherm models for nitrate adsorption of WM and WM@ZrO₂, including Langmuir, Freundlich, Sips, and Redlich-Peterson models (For interpretation of the references to color in this figure legend, the reader is referred to the Web version of this article).

owing to the low solubility of N₂ in water (Battino et al., 1984). Herein, adsorption performance was enhanced in response to an increased pyrolysis temperature since hard-carbon components remained after eliminating progressively soft-carbon components, indicating that the organic matters were decomposed of the biochar (Chen and Chen 2009).

EDS spectra (Fig. 6a) describe a semiquantitative analysis of inorganic elements obtained in biochar, including sodium (Na), magnesium (Mg), phosphorus (P), silicon (Si), chlorine (Cl), potassium (K), and calcium (Ca). In addition, EDS elemental mapping indicated that the main element was Ca, then followed by K, Cl, Na, Si, and trace amounts of Mg on the surfaces of biochar. These results were in good agreement with the major components of any biomass (Smith and White 2004). As shown in EDS spectra in Fig. 6b, biochar was rich in carbon with the highest proportions of carbon and oxygen. Interestingly, the presence of the N element in biochar after being treat-

Table 2 Parameters of kinetics for the nitrate adsorption onto WM and WM@ZrO₂.

Model	Unit	WM	WM@ZrO ₂
Pseudo- First-Order			
q_e	mg g ⁻¹	3.343	12.278
k_1	L mg ⁻¹	0.094	0.162
R^2	–	0.975	0.991
χ^2	–	0.019	0.031
Pseudo-Second-Order			
q_e		3.808	13.519
k_2	L ^{1/n} mg ^{1-1/n} g ⁻¹	0.034	0.019
R^2	–	0.990	0.998
χ^2	–	0.035	0.163
Intra-particle diffusion			
k_{IP}	mg g ⁻¹ min ^{-1/2}	0.112	0.001
C	mg g ⁻¹	9.12	12.297
R^2	–	0.953	0.976
χ^2	–	0.156	0.156
Elovich			
α	mg g ⁻¹ min ⁻¹	1.612	47.355
β	g mg ⁻¹	1.463	0.578
R^2	–	0.941	0.957
χ^2	–	0.083	0.817

Table 3 Parameters of isotherm for the nitrate adsorption onto WM and WM@ZrO₂.

Model	Unit	WM	WM@ZrO ₂
Langmuir			
q_m	mg g ⁻¹	4.069	15.196
k_L	L mg ⁻¹	0.054	0.053
R^2	–	0.972	0.985
R_L (*)	–	0.480	0.485
χ^2	–	0.049	0.351
Freundlich			
k_F	L ^{1/n} mg ^{1-1/n} g ⁻¹	0.771	2.732
n_F	–	3.019	2.924
R^2	–	0.931	0.954
χ^2	–	0.122	1.087
Sips			
q_m	mg g ⁻¹	3.229	15.121
k_S	L mg ⁻¹	0.082	0.014
n_S	–	0.005	0.003
R^2	–	0.983	0.981
χ^2	–	0.159	0.631
Redlich-Peterson			
k_{RP}	L g ⁻¹	2.489	55.338
α_{RP}	(mg L) ^{-g}	0.076	0.011
C_s^g	–	0.668	1.273
R^2	–	0.931	0.991
χ^2	–	0.147	0.221

(*) R_L was obtained from the Dimensionless constant separation factor by Hall et al. (Hall et al., 1966).

ted with nitrate indicated that nitrate was adsorbed onto the surface of biochar in Fig. 6b. Moreover, EDS results depict the appearance of Zirconium (Zr), confirming that ZrO₂ NPs were modified successfully onto the surface of WM@ZrO₂.

XRD analysis is an effective characterization technique for identifying the amorphous or crystalline in the adsorbent. Fig. 7a illustrates the XRD patterns of WM (α) and

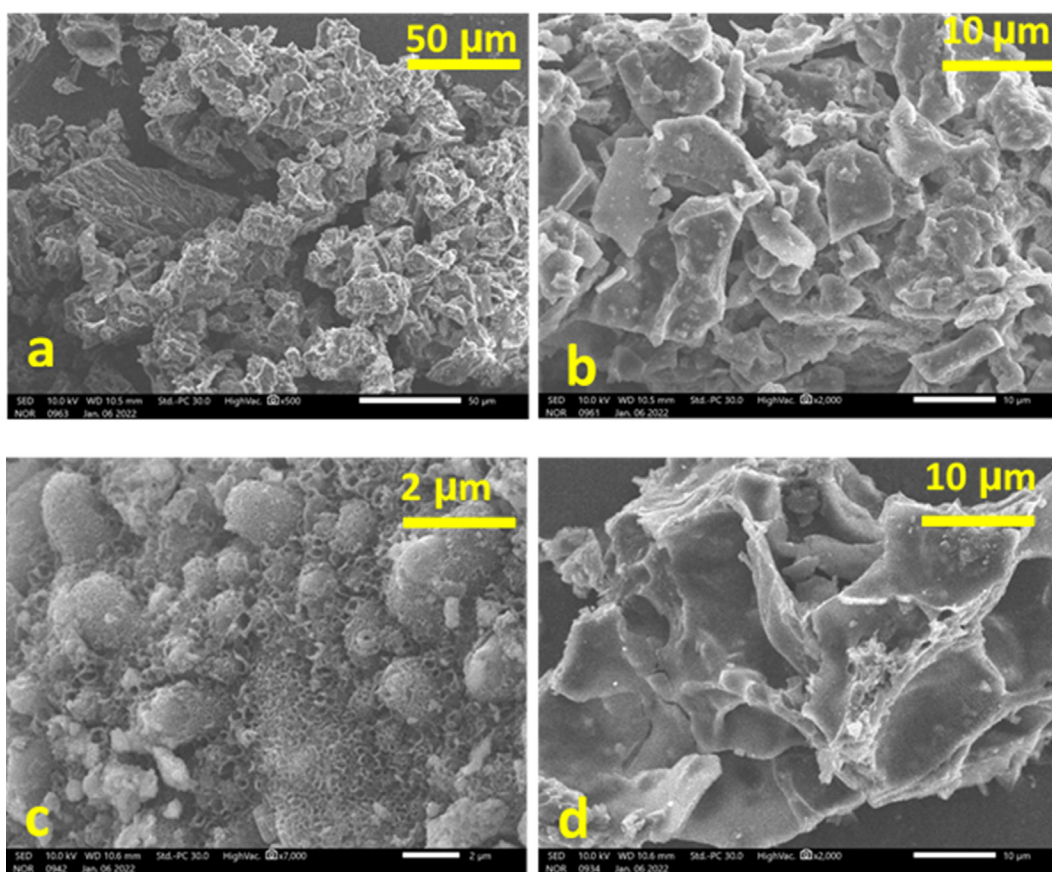


Fig. 5 Scanning electron micrograph (SEM) of biochar before (a), (b) and after (c), (d) nitrate adsorption. The corresponding X-ray energy dispersive spectra (EDS) of the red selected region of biochar.

WM@ZrO₂ (β). The XRD spectrum depicts two major diffraction peaks, which can be corresponded with the crystal plane for quartz (JCPDS PDF No. 39–1425) and calcite (JCPDS 5–586) in both samples. This finding was consistent with the previous report that the majority of crystalline belonged to quartz and calcite on biochar (Gupta and Mondal 2020). In addition, the XRD patterns of WM@ZrO₂ presented diffraction peaks of the monoclinic structure of ZrO₂ (JCPDS 37–1484), indicating the success of ZrO₂ NPs coating onto the surface of the adsorbent. The small characteristics of the board peak were observed at 23° for both samples, which were assigned to C(002) diffraction of parallel and azimuthal orientation of the aromatic and carbonized structure as a graphitized carbon with an amorphous framework (Demir et al., 2015, Yan et al., 2021).

The infrared absorption spectroscopy, which involves the vibrations in the dominant functional groups, indicates the nitrate adsorption on the surface of WM@ZrO₂. Fig. 7b depicts the FTIR spectrum of biochar before and after nitrate adsorption. The band at 3441 cm⁻¹ was considered the stretching vibration of the O–H group of water and hydrogen bound O–H groups in the layers and interlayer water molecules (Wang et al., 2007). Additionally, the band with a peak at 2920 and 2854 cm⁻¹ can be ascribed to stretching vibration of C–H and –CH₂, respectively (Antonangelo et al., 2019, Reza et al., 2020). The band with a peak at 2366 cm⁻¹ can be attributed to C≡C stretching vibrations. Besides, the

absorption band at 1630 cm⁻¹ was accounted for the stretching vibration of aromatic C = C and C = O in biochar (Popescu et al., 2007). As shown in Fig. 7b, the FTIR spectrum of biochar after nitrate adsorption featured the band at 1360 cm⁻¹ and 835 cm⁻¹ in the spectra were attributed to the –NO₃ stretching, indicating that the presence of nitrate after adsorption is closely related to the features of a –NO₃ group on the surface of biochar (Wang et al., 2004). In addition, vibrations at 1074 and 1053 cm⁻¹ can be assigned to the C–O stretching before and after nitrate adsorption, respectively. The shift of C–O peaks is responsible for aromatization obtained as the pyrolysis temperature increases (Li et al., 2016). This result indicates effective adsorption for trapping the nitrate on the surface of WM@ZrO₂.

Fig. 7c illustrates the pHPZC of WM and WM@ZrO₂, and their values were 9.52 and 8.89, respectively. For WM, as pH was < 9.52 (pH < pHPZC), the adsorbent was predominantly positively charged, favouring the affinity to adsorb the negatively charged nitrate anions by electrostatic attraction. In terms of WM@ZrO₂, the pHPZC was decreased due to the presence of ZrO₂ nanoparticles on the surface of biochar. This behavior was consistent with a previous study by Zhang et al. (Zhang et al., 2020). All adsorption nitrate processes occurred under acidic conditions; then, the nitrate anions electrostatically attracted to the WM@ZrO₂ surface. The surface charge of biochars was found to be pH-dependent due to the amphoteric nature of surface functional groups. The surface charge

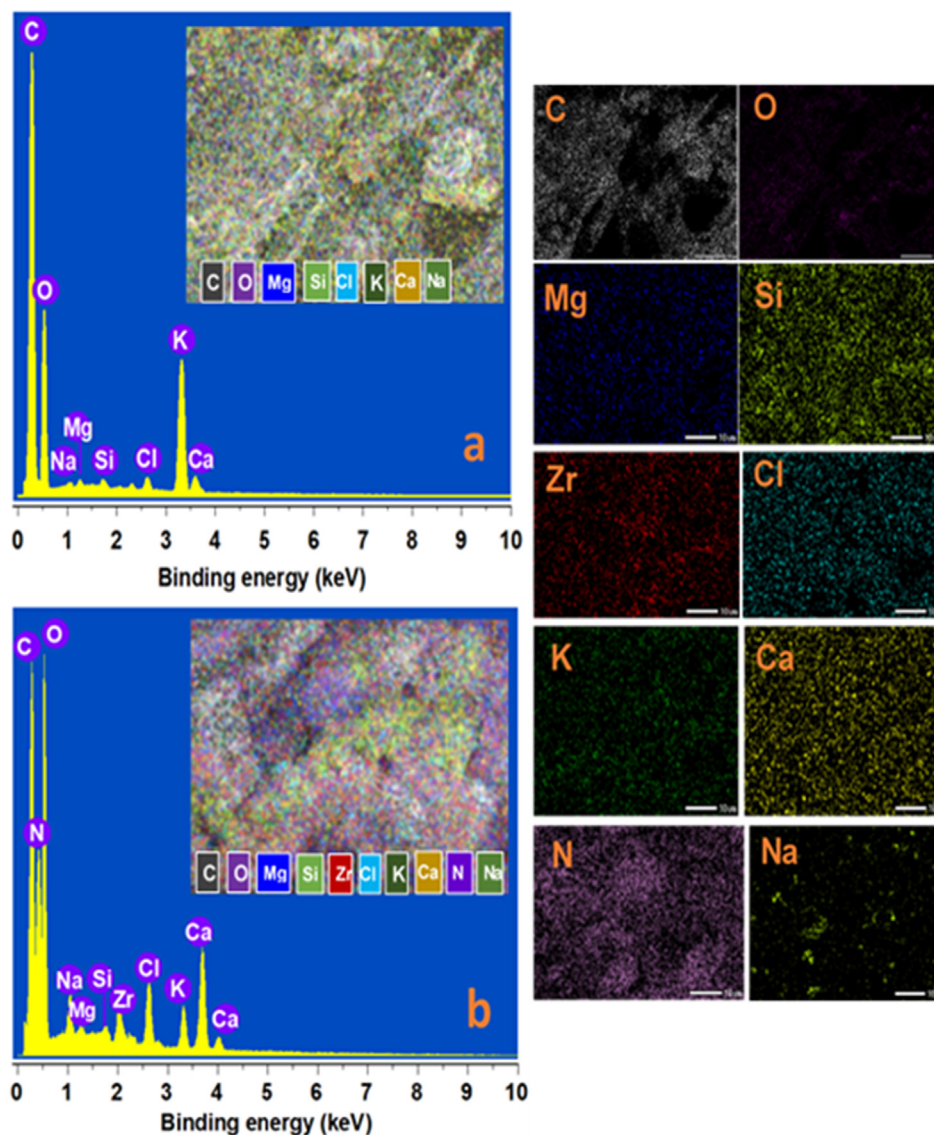


Fig. 6 The corresponding X-ray energy dispersive (EDS) spectra of biochar before (a), and after (b) nitrate adsorption. The mapping analysis of biochar before and after nitrate adsorption, indicates the mainly heterogeneous distribution of C, N, O, Mg, Si, P, Cl, Ca, and K (scale bar, 10 μm). (For interpretation of the references to color in this figure legend, the reader is referred to the Web version of this article.).

with the acid-base properties may be ascribed to the electrostatic attraction on the surface of biochar. Therefore, WM@ZrO₂ could have a high adsorption capacity on anionic nitrate at pH 2.

The mechanism of WM@ZrO₂ could be proposed for two main mechanisms, including electrostatic attraction and ligand exchange. Firstly, the WM@ZrO₂ was positively charged at pH < 8.89 and attracted nitrate anions onto the surface of WM@ZrO₂ by electrostatic attraction. Thus, the stronger acidic conditions could be more positive, which resulted in higher nitrate adsorption. This result also was consistent with the previous research by Apte et al. that the more phosphate anions were adsorbed, the more positive zeta potential under lower acidic conditions (Apte et al., 2007). Moreover, ligand exchange occurred between hydroxyl on the surface of biochars and nitrate anions from an aqueous solution. The -OH

groups on the surface of biochars were discussed in FTIR results and likely confirmed that the monolayer chemical identified the hydroxyl groups in nitrate adsorption. Therefore, the proposed mechanism of WM@ZrO₂ may mainly include electrostatic attraction and ligand exchange for nitrate adsorption. The mechanism of nitrate adsorption is illustrated in Fig. 8a.

3.7. Regeneration

The regeneration of WM@ZrO₂ with nitrate adsorption was tested to assess the reusability of biochar. Fig. 8b presents the nitrate adsorption of reusable WM@ZrO₂, which was carried out properly by chemical treatment. After five cycles, the nitrate adsorption remained > 50 % of the original adsorption capacity. It can be explained that the loss of the active sites in

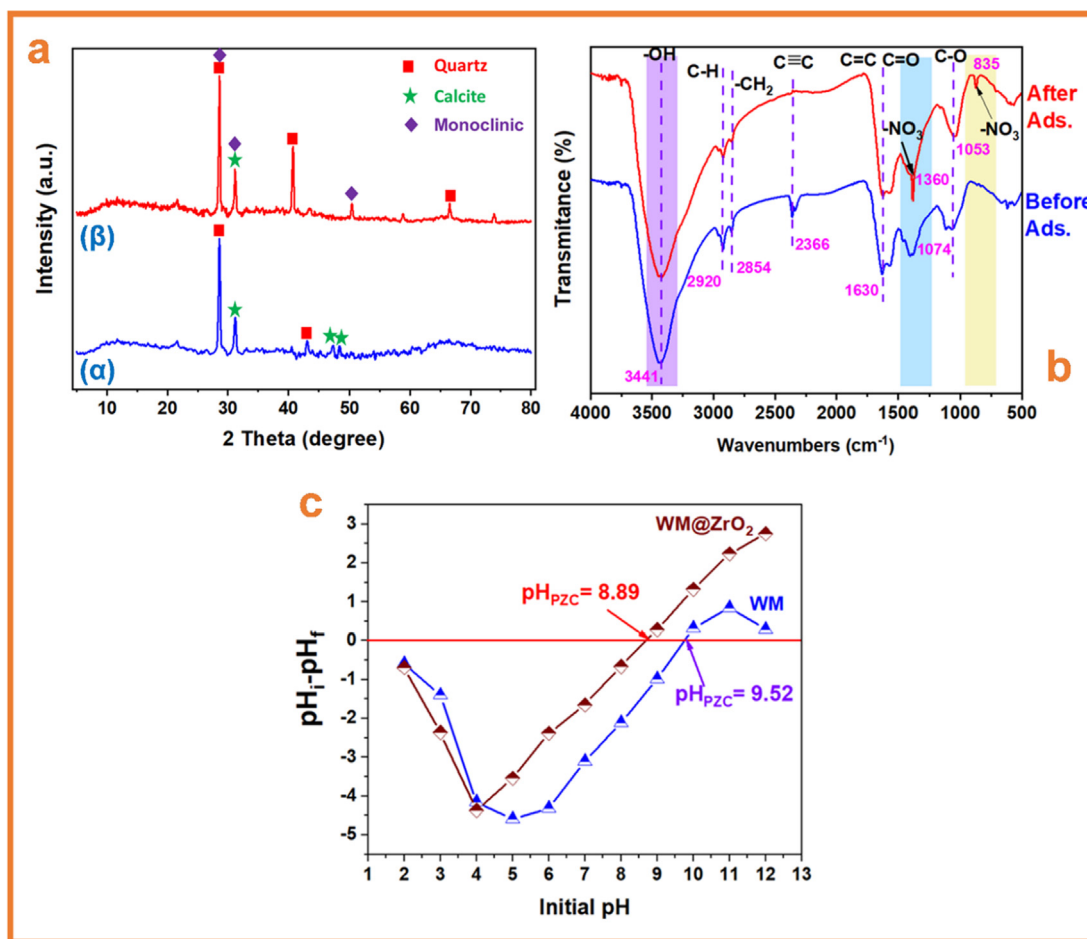


Fig. 7 (a) The XRD pattern of WM (α) and WM@ZrO₂ (β). (b) FTIR spectra of biochars before and after nitrate adsorption. (c) pHPZC of WM and WM@ZrO₂ (For interpretation of the references to color in this figure legend, the reader is referred to the Web version of this article).

adsorbents resulted in a decrease in the performance of adsorption capacity. As a result, WM@ZrO₂ was identified as the potential adsorbents for nitrate removal from an aqueous solution.

3.8. Real sample experiment

To test the applicability of WM@ZrO₂ for remediating contaminated water, the actual sample was collected from domestic wastewater. Before starting the experiment, all samples were filtered through a 0.45 μm membrane filter. The adsorption experiment was conducted with 0.6 g L⁻¹ of WM@ZrO₂. Then was shaken for 30 min at ambient temperature. The initial nitrate concentration, pH, total hardness, and total dissolved solids were 21 mg L⁻¹, 5.9, 1022 mg CaCO₃ L⁻¹, and 798 mg L⁻¹, respectively. After the adsorption experiment, the removal of nitrate for WM@ZrO₂ was achieved at 78 %, which was equivalent to the adsorption capacity of 8.1 mg g⁻¹ of adsorbent.

Watermelon rinds used as biochar has its a low cost due to solid wastes or agricultural wastes, resulting in the lower cost of biochar. Many studies reported that the price of modified biochar is about half of the activated carbon (Fdez-Sanromán et al., 2020). Herein, the utilization of solid wastes to synthesize

biochar in this study may not only save the cost of production, but also contribute to the environmental aspect of sustainable development. In addition, to test the feasibility of biochar, the nitrate adsorption capacity of WM@ZrO₂ was compared with those of other adsorbents as displayed in Table 4. Table 4 indicated that the nitrate adsorption capacity of this study could be comparable with that of wheat straw (WS) biochar reported by Xue et al. (Xue et al., 2016), lower than that of Ammonium-functionalized mesoporous silicas (AMS) (Saad et al., 2008) and Sugarcane bagasse (Hafshejani et al., 2016), but higher than that of other adsorbents including Oak sawdust biochar (OS) (Wang et al., 2015), Bamboo powder biochar (BP) (Mizuta et al., 2004), Pinewood biochar (PW) (Vijayaraghavan and Balasubramanian 2021), Microfibrillated cellulose modified with carbonated hydroxyapatite (MC) (Hokkanen et al., 2014), HTDMA modified Queensland bentonite (HTDMA) (Xi et al., 2010), pinewood residue biochar (PWR) (Chintala et al., 2013), and a broad range of biomass (BRB) (Zhang et al. (2020)). Therefore, in comparison with other adsorbents, WM@ZrO₂ was low in cost, environmentally friendly, and had a significantly high capacity for the removal of nitrate in aqueous media.

For the development of adsorbent research, the modification of biochar, the effect of adsorption, and the mechanism

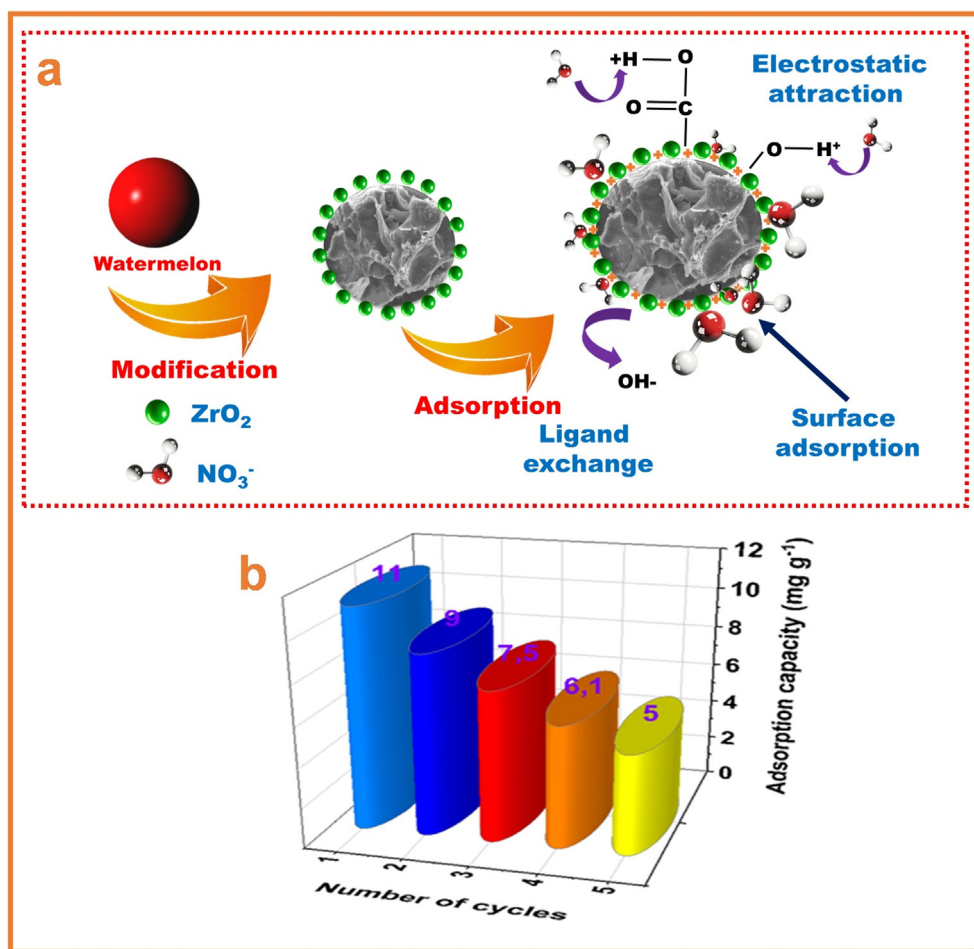


Fig. 8 (a) The mechanism of nitrate adsorption with WM@ZrO₂. (b) The adsorption capacity of WM@ZrO₂ in five cycles.

Table 4 Comparison of the nitrate adsorption capacity onto various adsorbents.

Adsorbent	pH	Initial concentration (mg L ⁻¹)	Adsorbent (g L ⁻¹)	Time (min)	q _{max} (mg g ⁻¹)	Ref.
Oak sawdust biochar	–	20	2	30	2.81	(Wang et al., 2015)
Bamboo powder biochar	–	10	1.25	–	5.54	(Mizuta et al., 2004)
Pinewood biochar	2.0	60	2.5	360	4.16	(Vijayaraghavan and Balasubramanian 2021)
Microfibrillated cellulose modified with carbonated hydroxyapatite	5.0	353	3.4	2400	12.96	(Hokkanen et al., 2014)
HTDMA modified Queensland bentonite	5.4	100	5	–	14.76	(Xi et al., 2010)
Wheat straw biochar	–	50	2	1500	24.8	(Xue et al., 2016)
Ammonium-functionalized Mesoporous silicas	–	130	1.0	180	46.5	(Saad et al., 2008)
Pinewood residue biochar	4.0	80	25	58	9.74	(Chintala et al., 2013)
Sugarcane bagasse	3.0	50	2	60	28.21	(Hafshejani et al., 2016)
A broad range of biomass	3.0	–	–	–	7.12	(Zhang et al. (2020))
Watermelon rind@ZrO ₂	2.0	60	1.0	60	15.20	This study

need to be fully addressed in future works. Especially, the improvement of preparation of biochar could be focused on. The development of modified biochar with high adsorption capacities to adsorb nitrate needs more in-depth research. Furthermore, the utilization of environmentally friendly and low-cost adsorbents needs to be tested further with different solid

wastes such as red mud, fly ash, agriculture wastes, etc. In the future, it is also possible to consider the aspect of improving optimal pH for WM@ZrO₂ in neutral conditions due to pH in reality conditions, such as water bodies. In summary, the prospects of WM@ZrO₂ as modified biochar with nitrate from contaminated water are fully promising.

4. Conclusions

In overall conclusion, we developed a method for synthesis of WM in which derived from watermelon rind. Based on our results, we demonstrated that loading the amount of ZrO₂ onto biochar may efficiently remove anionic nutrients, such as nitrate in an aqueous solution. The results indicated that WM as unmodified biochar was poor in the nitrate adsorption, whereas the modification of biochar may significantly enhance the nitrate adsorption capacity. The WM@ZrO₂ was characterized by BET, SEM, and EDS with mapping analysis, FTIR, and XRD to figure out the structure and composition of the adsorbent. For the Langmuir isotherm model, the maximum adsorption capacity was 15.196 mg g⁻¹. The adsorption isotherm was best fitted with the Langmuir model, highlighting the monolayer adsorption at homogeneous adsorption sites at the outer surface of the adsorbent. In addition, the reusability of WM@ZrO₂ was five cycles with relatively high performance in terms of adsorption capacity. The proposed mechanism, including electrostatic attraction and ligand exchange, played a dominant role in nitrate adsorption. The results from the actual sample experiment highlighted the use of WM@ZrO₂ as a promising adsorbent for application in water contaminated with nitrate. The challenges should be taken into consideration in the assessment of the environmental risk of biochar and the feasibility of its application. These results suggested that WM@ZrO₂ offered a promising, low-cost, environmentally friendly, and effective adsorbent to remove nitrate from an aqueous medium.

Declaration of Competing Interest

The authors declare that they have no known competing financial interests or personal relationships that could have appeared to influence the work reported in this paper.

Acknowledgements

The authors wish to acknowledge the precious help of Dr. Phuong Quynh Bui Thi, and Dr. Lan Huong Nguyen, for their kind collaborations. The authors also thank the support under the grant number of MOST 110-2221-E-006 -217 -MY3 (the Ministry of Science and Technology, Taiwan)

References

- Alagarsamy, A., Chandrasekaran, S., Manikandan, A., 2022. Green synthesis and characterization studies of biogenic zirconium oxide (ZrO₂) nanoparticles for adsorptive removal of methylene blue dye. *J. Mol. Struct.* 1247, 131275.
- Almaroai, Y.A., Usman, A.R., Ahmad, M., et al, 2014. Effects of biochar, cow bone, and eggshell on Pb availability to maize in contaminated soil irrigated with saline water. *Environ. Earth Sci.* 71, 1289–1296.
- Antonangelo, J.A., Zhang, H., Sun, X., et al, 2019. Physicochemical properties and morphology of biochars as affected by feedstock sources and pyrolysis temperatures. *Biochar.* 1, 325–336.
- Apte, S., Naik, S., Sonawane, R., et al, 2007. Synthesis of nanosized-necked structure α - and γ -Fe₂O₃ and its photocatalytic activity. *J. Am. Ceram. Soc.* 90, 412–414.
- Battino, R., Rettich, T.R., Tominaga, T., 1984. The solubility of nitrogen and air in liquids. *J. Phys. Chem. Ref. Data* 13, 563–600.
- Chen, B., Chen, Z., 2009. Sorption of naphthalene and 1-naphthol by biochars of orange peels with different pyrolytic temperatures. *Chemosphere* 76, 127–133.
- Chen, W., Luan, J., Yu, X., et al, 2020. The preparation of novel mineral-based mesoporous microsphere by microencapsulation technology and its application in the adsorption of dye contaminants. *Water Sci. Technol.* 81, 985–999.
- Chen, T., Zhang, S., Yuan, Z., 2020. Adoption of solid organic waste composting products: A critical review. *J. Clean. Prod.* 272, 122712.
- Chintala, R., Mollinedo, J., Schumacher, T.E., et al, 2013. Nitrate sorption and desorption in biochars from fast pyrolysis. *Micropor. Mesopor. Mater.* 179, 250–257.
- Cuixia, Y., Yingming, X., Lin, W., et al, 2020. Effect of different pyrolysis temperatures on physico-chemical characteristics and lead (ii) removal of biochar derived from chicken manure. *RSC Adv.* 10, 3667–3674.
- Dai, Y., Sun, Q., Wang, W., et al, 2018. Utilizations of agricultural waste as adsorbent for the removal of contaminants: a review. *Chemosphere* 211, 235–253.
- Demir, M., Kahveci, Z., Aksoy, B., et al, 2015. Graphitic biocarbon from metal-catalyzed hydrothermal carbonization of lignin. *Ind. Eng. Chem. Res.* 54, 10731–10739.
- Fan, S., Sun, Y., Yang, T., et al, 2020. Biochar derived from corn stalk and polyethylene co-pyrolysis: characterization and Pb (ii) removal potential. *RSC Adv.* 10, 6362–6376.
- Fdez-Sanromán, A., Pazos, M., Rosales, E., et al, 2020. Unravelling the environmental application of biochar as low-cost biosorbent: a review. *Appl. Sci.* 10, 7810.
- Guo, D., Hu, M., Chen, Z., et al, 2020. Catalytic Pyrolysis of rain tree biomass with nano nickel oxide synthesized from nickel plating slag: a green path for treating waste by waste. *Bioresour. Technol.* 315, 123831.
- Gupta, S.K., Gupta, R., Gupta, A., et al, 2000. Recurrent acute respiratory tract infections in areas with high nitrate concentrations in drinking water. *Environ. Health Perspect.* 108, 363–366.
- Gupta, G.K., Mondal, M.K., 2020. Mechanism of Cr (VI) uptake onto sagwan sawdust derived biochar and statistical optimization via response surface methodology. *Biomass Convers. Biorefin.* 1–17
- Hafshejani, L.D., Hooshmand, A., Naseri, A.A., et al, 2016. Removal of nitrate from aqueous solution by modified sugarcane bagasse biochar. *Ecol. Eng.* 95, 101–111.
- Hall, K.R., Eagleton, L.C., Acrivos, A., et al, 1966. Pore-and solid-diffusion kinetics in fixed-bed adsorption under constant-pattern conditions. *Ind. Eng. Chem. Fundam.* 5, 212–223.
- He, J., Lin, R., Long, H., et al, 2015. Adsorption characteristics of amino acids on to calcium oxalate. *J. Colloid Interface Sci.* 454, 144–151.
- Hokkanen, S., Repo, E., Westholm, L.J., et al, 2014. Adsorption of Ni²⁺, Cd²⁺, PO₄³⁻ and NO₃⁻ from aqueous solutions by nanostructured microfibrillated cellulose modified with carbonated hydroxyapatite. *Chem. Eng. J.* 252, 64–74.
- Jedynak, K., Szczepanik, B., Rędzia, N., et al, 2019. Ordered mesoporous carbons for adsorption of paracetamol and non-steroidal anti-inflammatory drugs: ibuprofen and naproxen from aqueous solutions. *Water* 11, 1099.
- Khadhri, N., M. E. K. Saad, M. ben Mosbah, et al., 2019. Batch and continuous column adsorption of indigo carmine onto activated carbon derived from date palm petiole. *Journal of Environmental Chemical Engineering.* 7, 102775.
- Kim, K.H., Kim, J.-Y., Cho, T.-S., et al, 2012. Influence of pyrolysis temperature on physicochemical properties of biochar obtained from the fast pyrolysis of pitch pine (*Pinus rigida*). *Bioresour. Technol.* 118, 158–162.
- Li, M., Feng, C., Zhang, Z., et al, 2010. Treatment of nitrate contaminated water using an electrochemical method. *Bioresour. Technol.* 101, 6553–6557.
- Li, Q., Li, X., Sun, J., et al, 2020. Removal of organic and inorganic matters from secondary effluent using resin adsorption and reuse of desorption eluate using ozone oxidation. *Chemosphere* 251, 126442.

- Li, G., Zhu, W., Zhang, C., et al, 2016. Effect of a magnetic field on the adsorptive removal of methylene blue onto wheat straw biochar. *Bioresour. Technol.* 206, 16–22.
- Liu, X., He, C., Yu, X., et al, 2018. Net-like porous activated carbon materials from shrimp shell by solution-processed carbonization and H₃PO₄ activation for methylene blue adsorption. *Powder Technol.* 326, 181–189.
- Liu, W.-J., Jiang, H., Yu, H.-Q., 2015. Development of biochar-based functional materials: toward a sustainable platform carbon material. *Chem. Rev.* 115, 12251–12285.
- Long, J., Yuvaraja, G., Zhou, S., et al, 2019. Inactive Fusarium Fungal strains (ZSY and MJY) isolation and application for the removal of Pb (II) ions from aqueous environment. *J. Ind. Eng. Chem.* 72, 442–452.
- Low, M., 1960. Kinetics of chemisorption of gases on solids. *Chem. Rev.* 60, 267–312.
- Luo, Z., Yao, B., Yang, X., et al, 2022. Novel insights into the adsorption of organic contaminants by biochar: a review. *Chemosphere* 287, 132113.
- Majumdar, D., Gupta, N., 2000. Nitrate pollution of groundwater and associated human health disorders. *Indian J. Environ. Health* 42, 28–39.
- Mizuta, K., Matsumoto, T., Hatate, Y., et al, 2004. Removal of nitrate-nitrogen from drinking water using bamboo powder charcoal. *Bioresour. Technol.* 95, 255–257.
- Popescu, C.-M., Popescu, M.-C., Singurel, G., et al, 2007. Spectral characterization of eucalyptus wood. *Appl. Spectrosc.* 61, 1168–1177.
- Prabhu, S.M., Pawar, R.R., Sasaki, K., et al, 2019. A mechanistic investigation of highly stable nano ZrO₂ decorated nitrogen-rich azacytosine tethered graphene oxide-based dendrimer for the removal of arsenite from water. *Chem. Eng. J.* 370, 1474–1484.
- Quang, H.H.P., Phan, K.T., Dinh, N.T., et al, 2022. Using ZrO₂ coated sludge from drinking water treatment plant as a novel adsorbent for nitrate removal from contaminated water. *Environ. Res.*, 113410
- Redlich, O., Peterson, D.L., 1959. A useful adsorption isotherm. *J. Phys. Chem.* 63, 1024.
- Reza, M.S., Islam, S.N., Afroze, S., et al, 2020. Evaluation of the bioenergy potential of invasive *Pennisetum purpureum* through pyrolysis and thermogravimetric analysis. *Energy, Ecol. Environ.* 5, 118–133.
- Saad, R., Hamoudi, S., Belkacemi, K., 2008. Adsorption of phosphate and nitrate anions on ammonium-functionalized mesoporous silicas. *J. Porous Mater.* 15, 315–323.
- Siddiqui, S.I., Chaudhry, S.A., 2019. Nanohybrid composite Fe₂O₃-ZrO₂/BC for inhibiting the growth of bacteria and adsorptive removal of arsenic and dyes from water. *J. Clean. Prod.* 223, 849–868.
- Sips, R., 1948. On the structure of a catalyst surface. *J. Chem. Phys.* 16, 490–495.
- Smith, F.A., White, J.W., 2004. Modern calibration of phytolith carbon isotope signatures for C₃/C₄ paleo-ecosystem reconstruction. *Palaeogeogr. Palaeoclimatol. Palaeoecol.* 207, 277–304.
- Tan, X., Liu, Y., Zeng, G., et al, 2015. Application of biochar for the removal of pollutants from aqueous solutions. *Chemosphere* 125, 70–85.
- Tanaka, S., Kano, S., Lat, J., et al, 2015. Effects of acacia mangium on morphological and physicochemical properties of soil. *J. Trop. For. Sci.*, 357–368
- Tyagi, S., Rawtani, D., Khatri, N., et al, 2018. Strategies for nitrate removal from aqueous environment using nanotechnology: a review. *J. Water Process Eng.* 21, 84–95.
- Varsha, M., Kumar, P.S., Rathi, B.S., 2022. A review on recent trends in the removal of emerging contaminants from aquatic environment using low-cost adsorbents. *Chemosphere* 287, 132270.
- Vijayaraghavan, K., Balasubramanian, R., 2021. Application of pine-wood waste-derived biochar for the removal of nitrate and phosphate from single and binary solutions. *Chemosphere* 278, 130361.
- Wang, B., Gao, B., Fang, J., 2017. Recent advances in engineered biochar productions and applications. *Crit. Rev. Environ. Sci. Technol.* 47, 2158–2207.
- Wang, Z., Guo, H., Shen, F., et al, 2015. Biochar produced from oak sawdust by Lanthanum (La)-involved pyrolysis for adsorption of ammonium (NH₄⁺), nitrate (NO₃⁻), and phosphate (PO₄³⁻). *Chemosphere* 119, 646–653.
- Wang, Y.M., Wu, Z.Y., Zhu, J.H., 2004. Surface functionalization of SBA-15 by the solvent-free method. *J. Solid State Chem.* 177, 3815–3823.
- Wang, X., Xi, G., Xiong, S., et al, 2007. Solution-phase synthesis of single-crystal CuO nanoribbons and nanorings. *Cryst. Growth Des.* 7, 930–934.
- Waqas, M., Aburizaiza, A., Miandad, R., et al, 2018. Development of biochar as fuel and catalyst in energy recovery technologies. *J. Clean. Prod.* 188, 477–488.
- Weber Jr, W.J., Morris, J.C., 1963. Kinetics of adsorption on carbon from solution. *J. Sanit. Eng. Div.* 89, 31–59.
- Wong, S., Lim, Y., Ngadi, N., et al, 2018. Removal of acetaminophen by activated carbon synthesized from spent tea leaves: equilibrium, kinetics and thermodynamics studies. *Powder Technol.* 338, 878–886.
- Xi, Y., Mallavarapu, M., Naidu, R., 2010. Preparation, characterization of surfactants modified clay minerals and nitrate adsorption. *Appl. Clay Sci.* 48, 92–96.
- Xue, L., Gao, B., Wan, Y., et al, 2016. High efficiency and selectivity of MgFe-LDH modified wheat-straw biochar in the removal of nitrate from aqueous solutions. *J. Taiwan Inst. Chem. Eng.* 63, 312–317.
- Yadav, S., Yadav, A., Bagotia, N., et al, 2021. Adsorptive potential of modified plant-based adsorbents for sequestration of dyes and heavy metals from wastewater-a review. *J. Water Process Eng.* 42, 102148.
- Yan, Y., Manickam, S., Lester, E., et al, 2021. Synthesis of graphene oxide and graphene quantum dots from miscanthus via ultrasound-assisted mechano-chemical cracking method. *Ultrason. Sonochem.* 73, 105519.
- Yu, M., Li, H., Li, K., et al, 2022. Magnetite-based biochar coupled with binary oxidants for the effective removal of mixed dye from wastewater. *Fibers Polym.* 23, 450–462.
- Zhang, H., Chen, C., Gray, E.M., et al, 2017. Effect of feedstock and pyrolysis temperature on properties of biochar governing end use efficacy. *Biomass Bioenergy* 105, 136–146.
- Zhang, L., Dan, H., Bukasa, O.T., et al, 2020. Low-cost efficient magnetic adsorbent for phosphorus removal from water. *ACS Omega* 5, 25326–25333.
- Zhang, M., Song, G., Gelardi, D.L., et al, 2020. Evaluating biochar and its modifications for the removal of ammonium, nitrate, and phosphate in water. *Water Res.* 186, 116303.
- Zhao, H., Li, Y., Song, Q., et al, 2019. Investigation on the thermal behavior characteristics and products composition of four pulverized coals: its potential applications in coal cleaning. *Int. J. Hydrogen Energy* 44, 23620–23638.
- Zhuang, S., Zhu, K., Xu, L., et al, 2022. Adsorption of Co²⁺ and Sr²⁺ in aqueous solution by a novel fibrous chitosan biosorbent. *Sci. Total Environ.* 825, 153998.
- Zong, E., Huang, G., Liu, X., et al, 2018. A lignin-based nano-adsorbent for superfast and highly selective removal of phosphate. *J. Mater. Chem. A* 6, 9971–9983.